Proceedings of the Estonian Academy of Sciences,
2017, **66**, 4, 422–429
https://doi.org/10.3176/proc.2017.4.19
Available online at www.eap.ee/proceedings

FUNCTIONAL MATERIALS

Raman spectral identification of phase distribution in anodic titanium dioxide coating

Ainars Knoks*, Janis Kleperis, and Liga Grinberga

Institute of Solid State Physics, University of Latvia, Kengaraga Str. 8, LV-1063 Riga, Latvia

Received 7 May 2017, revised 18 July 2017, accepted 22 August 2017, available online 30 November 2017

Abstract. Growing need for cleaner environment and energy production has brought about a hunt for perspective materials. One of such perspective materials is titanium dioxide (TiO_2, titania) due to its chemical stability and photocatalytic properties. Titania can be synthesized through many methods but anodization process is one of the prevailing methods to produce high active surface nanostructured titania. Various anodization electrolytes produce different polymorphs of TiO_2. Uniform phase distribution on the surface is crucial for higher photocatalytic activity. In this research, the influence of two electrolytes on polymorph phase distribution of TiO_2 was investigated. Phase distribution correlation with optical band gap, charge density and photocurrent values were tested. Successful Raman investigation of anodized titania revealed uniform, single and multi-phase, as well as nonuniform phase distributions produced respectively in PO_4^{3-} and SO_4^{2-} ions containing electrolytes. Uniform single phase titania shows highest photocurrent (PCR) and charge density values compared to phase composition and nonuniform phase distributions. We have shown Raman microprobe analysis as indispensable method for wholesome sample characteristics.

Key words: TiO_2, structure, anodization, Raman.

1. INTRODUCTION

In the world of an accelerated energy consumption [1] and generation [2] great amount of work is put in into investigation of reduction of the pollution from industry [1,3,4] as well as individual homes [5], to find most efficient way of energy usage and lower the levels of pollution, according to Paris Agreement [6]. A prevalent way to lower pollution is through photocatalytic reduction [7]. In materials with potential use for photocatalytic pollution degradation the most promising seems to be titanium dioxide (TiO_2, titania). It can be used for transformation of solar energy into chemical energy for splitting of water into hydrogen and oxygen [8], CO_2 reduction [9,10] and organic pollution degradation [7] as well as many other applications. The main advantage of TiO_2 is its chemical and photocatalytic stability, high availability, high oxidation potential of $^{\bullet}OH$ radicals and environmental acceptability. Even though the photocatalytic properties of TiO_2 were shown already 40 years ago by Fujishima and Honda [11] and many studies have been conducted, finding highly efficient material is still in progress. TiO_2 can be synthesized in anatase (A), rutile (R), and brookite polymorph forms as well as in forms of cubic, pyrite, monoclinic and cotunnite [12] through various methods: magnetron sputtering, electrochemical anodization, electrophoretic deposition, spray-pyrolysis etc. [13–15]. Most of amorphous coatings are produced using previously mentioned methods of synthesis. This means that heat treatment is necessary for crystalline structure. It is well known that rutile is thermodynamically stabile phase and anatase transforms into rutile at higher

* Corresponding author, ainars.knoks@gmail.com

calcination temperatures [16]. Phase transition depends on the synthesis method and calcination atmosphere, for example [17] reports no phase transition up to 873 K, but [16] showed 703 K as threshold temperature for transformation. Comprehensive table and graph on phase transition was reported by Hanaor et al. [12] suggesting A to R transformation in ambient atmosphere above 873 K, whereas Mor et al. [18] reported crystallization temperature as low as 553 K. It is necessary to find right calcination temperature for the synthesis method to ensure the desired polymorph phase composition as it influences the overall photocatalytic activity.

It has been reported that multiphase composition ensures higher photocatalytic activity [19]. The knowledge of polymorph phase structure distribution of TiO_2 coating is essential for more favourable optical and photocatalytic properties. Due to various possible outcomes of structural composition it is necessary to investigate the TiO_2 surface for polymorph phase distribution.

This research is focused on the investigation of influence of anodization properties on the phase uniformity of anodized TiO_2 coating on Ti foil. Investigation of TiO_2 surface morphology and polymorph phase is done by SEM and Raman spectroscopy. Correlation between optical absorption edge, charge carrier density and uniformity of phase distribution is reported.

2. MATERIALS AND METHODS

2.1. Experimental setup

Experimental setup as seen in Fig. 1 was used for sample synthesis. Titanium (Ti) foil was mechanically polished using chromium paste (particle size 0.25–1 μm) then sonicated (US) in acetone bath for 10 minutes. Additional chemical polishing with $HF:HNO_3:H_2O$ (volume relation 1:4:4) was performed for some samples. Cleaned Ti substrate was used as anode and platinum (Pt) as counter electrode. Electrolyte was under constant stirring throughout the process of the synthesis, current density on the surface as well as temperature were measured.

Two kinds of electrolytes were prepared. First, by dissolving H_3PO_4 (85%, Penta) in deionized (DI) water. Second, by dissolving H_2SO_4 in DI water. 1 M NaOH (Enola) was added to the solution to tweak the pH level to 2.5. Both electrolytes are water based, as Grimes et al [20] reported there is a need of F^- ion source, Regonini et al. [21] came to the same conclusions. To ensure anodic process by chemical dissolution of TiO_2 NaF (Enola) was added. Thus, F^- ion concentration of 0.3 wt% was ensured.

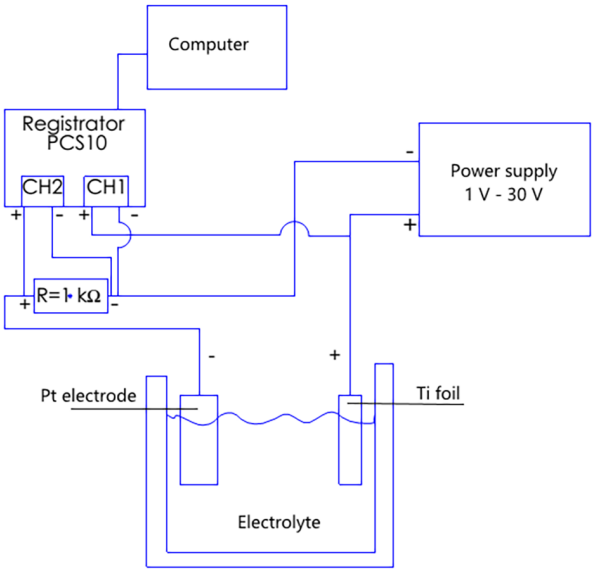

Fig. 1. Anodization setup for sample synthesis.

Anodizing current-time transient is shown in Fig. 2. As reported by [21] anodization process can be divided into 3 stages. Stage I, anodization process begins with applied voltage, TiO_2 layer grows on Ti substrate following drop of current density due to higher resistance. Though authors suggest extending phase I, with low voltage application before the anodization voltage, to ensure initial oxide layer, pH gradient and speed up anodization process in given electrolyte. In stage I the oxide layer thickens until the rapid pore evolution starts; in the stage II, chemical and field assisted etching of oxide layer proceeds and Ti^{4+} and O^{2-} ions migrate to oxide-electrolyte and metal-oxide interfaces; in stage III an equilibrium between oxide growth and dissolution

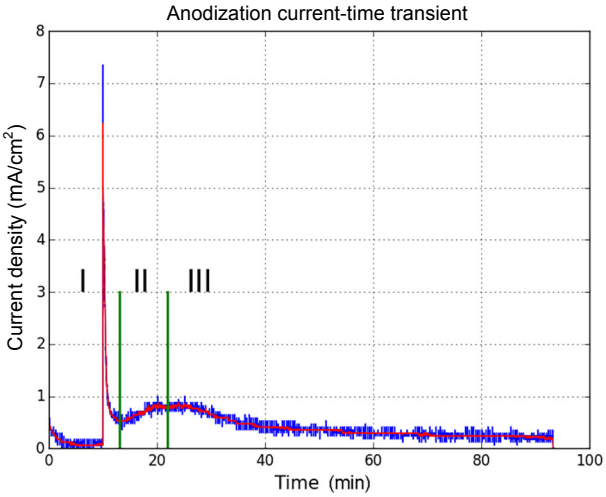

Fig. 2. Anodizing current-time transient.

(field assisted as well as chemical) is achieved and pores turn into tubes and oxide layer [21,22].

After anodization samples were rinsed in DI water and dried in ambient atmosphere. As anodized TiO_2 is amorphous crystalline structure of samples was achieved by heat treatment in ambient atmosphere at 773 K, except for one sample treated with heat in nitrogen atmosphere at 773 K.

Photoactivity was determined using three electrode cell, where sample was used as working electrode, Pt as auxiliary electrode and calomel (SCE) as the reference electrode, VoltaLab 40 (PGZ301, Radiometer Analytical) potentiostat was used. In photoactivity measurements 150 W xenon lamp (10 mW/cm^2) was applied as light source by cycled ON and OFF irradiation with self-made chopper.

In this work two sets of samples are compared; sample synthesis parameters are presented in Table 1.

3. RESULTS AND DISCUSSION

3.1. Morphology

If it is necessary to produce high specific area materials for higher efficiency of absorbed irradiation, nano-structured surface is the right answer. As seen in SEM investigation (Fig. 3) both electrolytes can produce nanotube structures of titania. But two problems arise: lack of uniformity of the tubular layer and anodization excess contamination, even though proper rinsing and annealing is performed. As seen in Fig. 3 (c) not only surface is semi-chaotic, meaning not clear tubular structure, but the surface can be contaminated with flower like structures.

On the other hand, tubular structure of Fig. 3 (a), (b), and (d) are partially covered with thin oxide layer, closing the openings of tubes.

3.2. Structural composition

Single spot spectroscopic investigation shows 3 various titania phase compositions as seen in Fig. 4 (a), (b) and (c) provides with various polymorph phase indications. Both most common polymorph phases are present. Anatase phase is characterized with major modes at 144, 196, 396, 515 and 632 cm^{-1} as seen in Fig. 4 (b). Other samples show mostly anatase phase as seen in Fig. 4 (c) with shifted multiphoton mode at 245 cm^{-1} and major R modes at 445 cm^{-1} and 613 cm^{-1}. Sample results seen in Fig. 4 (a) suggests mostly rutile structure with two anatase modes.

Table 1. Sample synthesis parameters. Two sets of samples were synthesized, differentiating in used electrolyte. TH represents H_3PO_4 and TS represents H_2SO_4 containing electrolyte

Sample	Chemical polishing, s	Low voltage, V	Time, min	Anodization voltage, V	Time, min	Electrolyte	Annealing atmosphere	T, K	Heat treatment time, min
TH1	0	5	10	20	90	H_3PO_4	Ambient	773	240
TH2	0	5	10	20	90	H_3PO_4	Nitrogen	773	120
TH3	1	5	10	20	90	H_3PO_4	Ambient	773	240
TH4	0	5	10	20	90	H_3PO_4	Ambient	773	120
TS1	5	5	10	20	90	H_2SO_4	Ambient	773	240
TS2	0	5	15	20	90	H_2SO_4	Ambient	773	240
TS3	5	5	15	20	90	H_2SO_4	Ambient	773	240

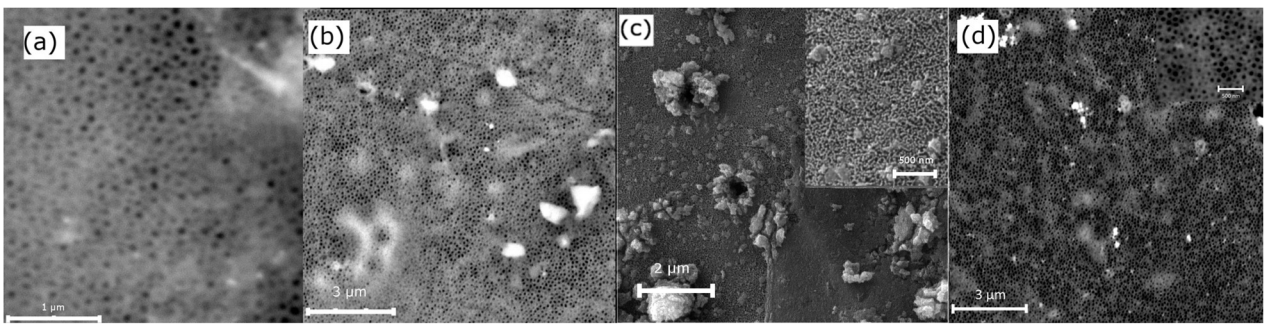

Fig. 3. Morphology investigation. (a) tubular structures of TiO_2 sample TH1; (b) tubular structure covered with anodization excess TH2; (c) microstructural surface contamination with TiO_2 flowers of TS3 (d) TiO_2 tubular structure TH4.

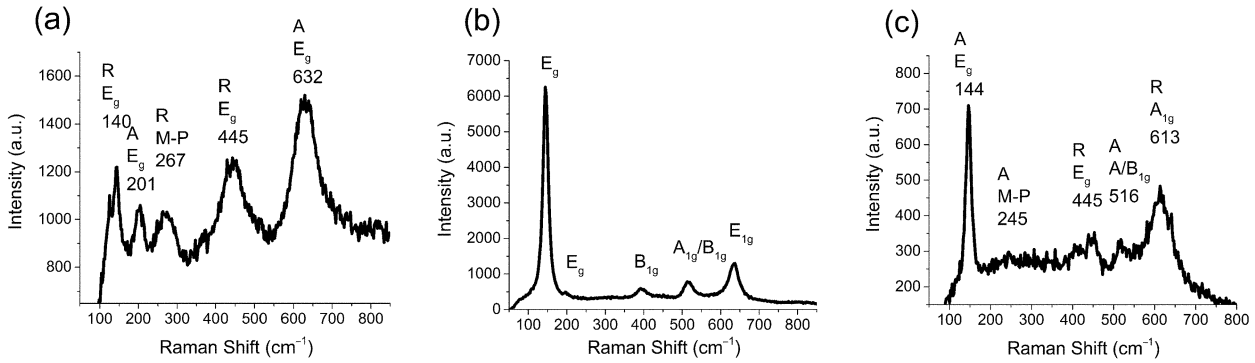

Fig. 4. Raman shift spectroscopy single spot investigation. (a) TH1 mostly Rutile phase; (b) TH2 pure single Anatase phase; (c) TS3 Anatase–Rutile composition with peak shifts.

For thorough surface characterization, it is necessary to map phase distribution on the surface by taking multiple spectra, results of multiple lines of spectra can be seen in Fig. 5. The phase distribution varies over the surface of different samples. Tubular structure (Fig. 5 (b)) shows uniform single phase surface in Fig. 5 (a). Uniform structural composition, although not of single phase, distribution seen in Fig. 5 (b), which morphology is with specific structure but not tubular as seen in Fig. 5 (c).

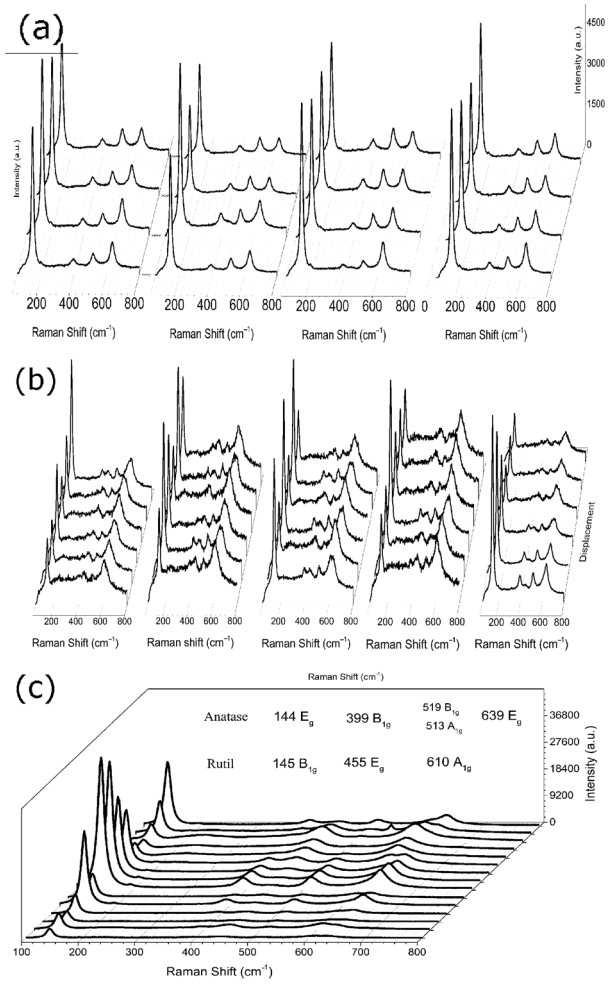

Fig. 5. Raman mapping of surface. (a) single anatase phase evenly distributed of TH2; (b) phase composition of anatase and rutile, semi-even distribution TS3; (c) TS1 anatase and rutile phase in separate positions.

For more comprehensive depiction of distribution, density plots of specific polymorph phase as seen in where color represents single spectra depending on co-ordinates can be seen in Fig. 6. As seen in Fig. 6 (a), (b), and (c) the surface has mostly uniform phase composition, density plots are in uniform color, but it must be kept in mind that in case of sample A, even though mostly uniform distribution, it is not single polymorph phase but phase composition as seen in Fig. 4 (a). In comparison to the sample TH2 where the surface is single polymorph phase with difference in acquired signal intensity, indicating slightly varying crystallite size. Whereas Fig. 6 (c) shows two phase composition in TS3, where green and red represents respectively rutile and anatase polymorph phases.

Distribution density plot of two single phases clearly can be seen in Fig. 7, where amongst rutile there is a small island of anatase. As seen from Fig. 7 (b) the anatase phase is just in one location. The single anatase island can be explained with higher number of defects due to TiO_2 layer cracking.

3.3. Optical properties

Optical absorption edge was determined from Kubelka–Munk function [23,24] applied to reflectance spectra and by linear fitting and extrapolating to maximum absorption. Keeping in mind theoretical calculated band gap values of rutile 3.05 eV [25] and anatase 3.2 eV [26], our results are anatase-rutile composition in TH1 (Fig. 5 (a)) $E_g = 3.2$ eV, TH2 uniform anatase phase (Fig. 5 (b)) $E_g = 3.3$ eV, but sample TS3 phase composition (Fig. 5 (c)) $E_g = 2.9$ eV. Aforementioned three electrode photo-electrochemical cell allows to measure

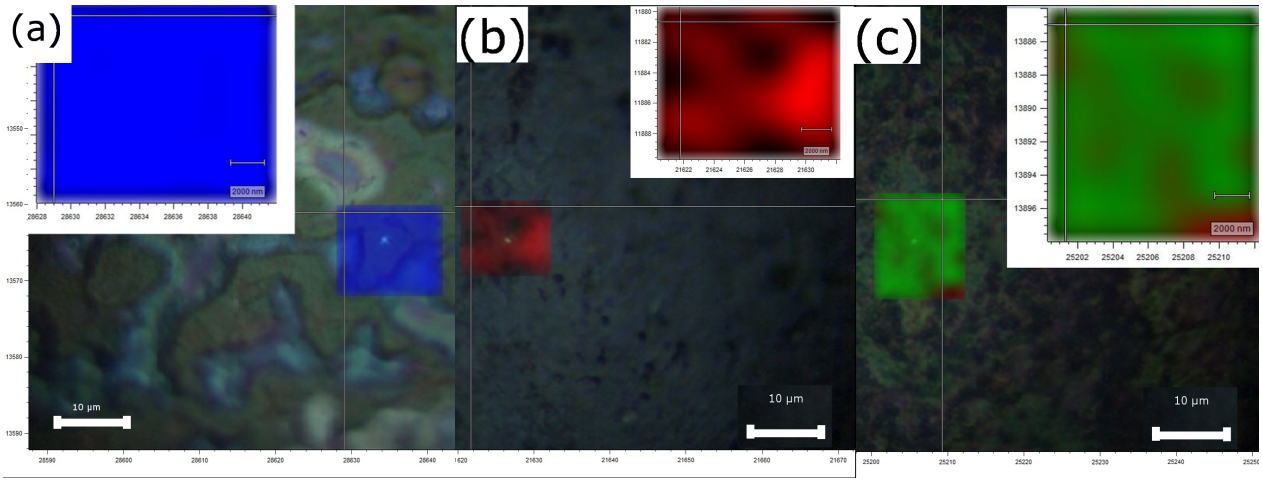

Fig. 6. Polymorph phase distribution on surface. Images consists of microscope image of sample surface in the background, scanned area is colored, phase distribution distinguished by intensity of colour. Blue – Rutile–Anatase phase composition seen in Fig. 4 (a); red – anatase phase seen in Fig. 4 (b); green – Rutile phase seen in Fig. 4 (c). (a) uniform distribution of phase composition; (b) uniform single phase distribution, dark spots are in same phase but with lower signal intensity; (c) semi uniform phase distribution of various crystalline phases.

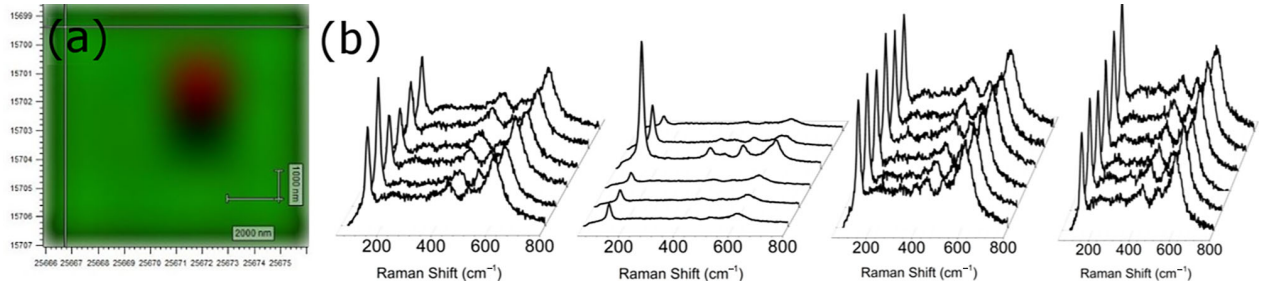

Fig. 7. Phase distribution density plot of TS2 (a) red color represents anatase phase, green represents rutile phase (b) phase distribution shown in Raman spectra, one anatase peak (red in (a)) in the middle of Rutile phase (green in (a)).

open circuit potential (OCP), which provides with rough determination of electron-hole generation and recombination rate, and photocurrent (PCR) which in turn provides with an estimates of amount of charge carriers. Fig. 8 (a) shows PCR value for TH1 uniform single anatase phase sample and Fig. 8 (b) TS3 OCP value of phase composition sample. From voltage-time transient we can estimate rough recombination rate, as seen in Fig. 8 (b), in 10 seconds potential difference of 15 mV then for next 50 seconds only 7 mV of increase in potential is created, thus showing the high recombination rate. Single phase distribution as seen in sample TH2 (Fig. 5 (a), Fig. 6 (b)) shows 8 µA/cm^2 whereas sample TH1 (rutile majority Fig. 4 (a)) shows 4 µA/cm^2. Even lower PCR values of 0.61 µA/cm^2 and 0.45 µA/cm^2 were shown by samples TS1 and TS2.

Efficient photocatalytic material requires high charge carrier density – N_D. N_D was determined by linear approximation of Mott–Schottky plot [27,28]. N_D estimate for nanotubular pure anatase phase (Fig. 5 (a)) sample TH2 is 2.8×10^{19} cm^{-3}, compared to TS2 nontubular nonuniform phase composition (Fig. 7) with mostly rutile polymorph N_D is 1.2×10^{19} cm^{-3}, and TS3 phase composition (seen in Fig. 4 (c) and Fig. 5 (b)) $N_D = 2.26 \times 10^{17}$ cm^{-3}. Whereas tubular anatase TH4 N_D estimated to 4.6×10^{22} cm^{-3}. Samples synthesized in H_3PO_4 electrolyte flat band potentials are below –1 V but other samples synthesized in H_2SO_4 based electrolyte flat band potentials over –2 V and N_D lower by 2 to 3 orders of magnitude. Comparing samples TH2 and TS3 respectively flat band potential were –0.57 V and –2.2 V.

As seen in Table 2 samples synthesized in H_3PO_4 showed higher band gap, PCR and N_D values, whereas samples synthesized in H_2SO_4 showed lower band gap, PCR and N_D values. TS samples show lower E_{gap} values that corresponds well with structrual properties, as rutile

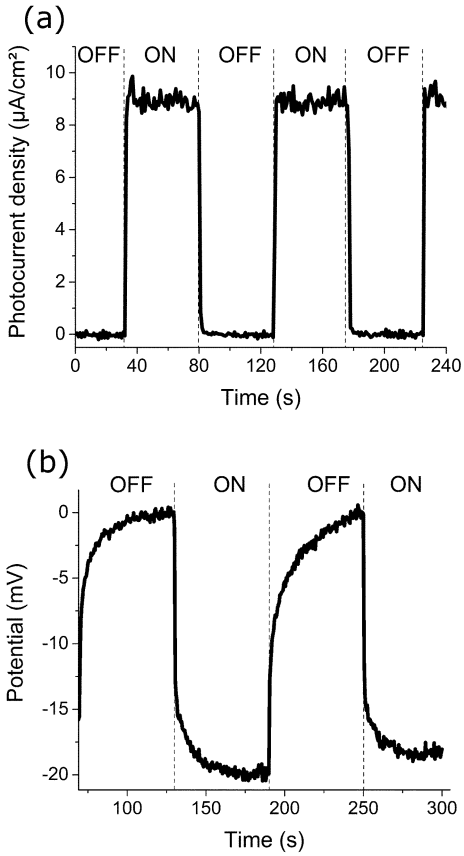

Fig. 8. Potential-time transient (OCP) and photocurrent-time transient (PCR) graphs. (a) Sample TH2 PCR value of single phase uniform distribution of anatase; (b) TS3 phase composition OCP value of –22 mV.

phase has lower band gap values, but also TS show lower PCR values that translates into lower overall photo-activity. Similarly high E_{Fb} assits in confirming lower activity, all samples with very high flat band potentials show lower activity. Additionally, heat treatment environment is crucial for higher activity as it is well seen for sample TH2 and TH4, single anatase phase, low E_{Fb} value, high activity.

4. CONCLUSIONS

In this research anodized titania was synthesized in two different electrolytes and optical, structural and electrochemical properties were tested with main attention to polymorph phase distribution of samples with 2D Raman investigation.

Considering the synthesis parameters and anatase to rutile transformation parameters in comparison with the results presented here, conclusions on the electrolyte influence on crystallinity of TiO_2 can be made. Uniform and mostly anatase phase samples were synthesized using H_3PO_4 based electrolyte whereas mostly rutile distribution was achieved with H_2SO_4 based electrolyte with similar synthesis and heat treatment parameters. Anodized TiO_2 surface phase distribution depends on anodization electrolyte as well as heat treatment temperature and sample preparation for anodization, as it was showed by Raman individual and phase distribution plots.

Phase distribution has direct influence on overall photocatalytic activity of TiO_2 influencing charge carrier density and recombination rate. There was no observed correlation between multiphase composition and higher charge carrier densities, higher PCR values. With the right choice of electrolyte and heat treatment atmosphere it is possible to ensure higher photoactivity.

By combining TiO_2 polymorph phase distribution with PCR values and charge carrier densities we present novel method of estimation of material overall photoactivity. Because of the major differences in phase composition, the surface analysis is necessary and Raman microprobe analysis is indispensable method for wholesome sample surface characterization.

Table 2. Measurement results for all samples

Sample	OCP, mV	FCR, $\mu A/cm^2$	E_{gap}, eV	Polymorph phase	E_{Fb}, mV	N_D, m^3
TH1	–7.47	4.00	3.20	R	1395.5	2.41E+17
TH2	–300.15	8.20	3.30	A	–572.6	2.78E+19
TH3	–8.64	0.02	2.99	A/R	–1246.6	1.96E+23
TH4	–80.00	5.62	3.11	A	–646.3	4.63E+22
TS1	–0.49	0.45	2.94	R/A	–2124.6	7.64E+15
TS2	–9.42	0.61	2.99	R/A	–6253.3	1.23E+19
TS3	–22.07	0.81	2.90	R/A	–2182.8	2.27E+17

ACKNOWLEDGEMENTS

Authors acknowledge National Research Programs IMIS[2] and LATENERGI. The publication costs of this article were covered by the Estonian Academy of Sciences and the University of Tartu.

REFERENCES

1. Dai, Y. and Gao, H. O. Energy consumption in China's logistics industry: A decomposition analysis using the LMDI approach. *Transp. Res. Part D Transp. Environ.*, 2016, **46**, 69–80.
2. International Energy Agency. *Key world energy statistics*. 2016.
3. Xu, B. and Lin, B. Assessing CO_2 emissions in China's iron and steel industry: a dynamic vector autoregression model. *Appl. Energy*, 2016, **161**, 375–386.
4. Lin, B. and Xie, C. Reduction potential of CO_2 emissions in China's transport industry. *Renew. Sustain. Energy Rev*. 2014, **33**, 689–700.
5. Geng, C., Chen, J., Yang, X., Ren, L., Yin, B., Liu, X., et al. Emission factors of polycyclic aromatic hydrocarbons from domestic coal combustion in China. *J. Environ. Sci*., 2014, **26**(1), 160–166.
6. Communication from the Commission to the European Parliament, the Council, the European Economic and Social Committee and the Committee of the Regions: a European Strategy for Low-Emission Mobility. European Commission, Brussels, 2016, SWD (2016) 244.
7. Chatterjee, D. and Dasgupta, S. Visible light induced photocatalytic degradation of organic pollutants. *J. Photochem. Photobiol. C Photochem. Rev*., 2005, **6**(2–3), 186–205.
8. Kmentova, H., Kment, S., Wang, L., Pausova, S., Vaclavu, T., Kuzel, R., et al. Photoelectrochemical and structural properties of TiO_2 nanotubes and nanorods grown on FTO substrate: Comparative study between electrochemical anodization and hydrothermal method used for the nanostructures fabrication. *Catal. Today*, 2016, **287**, 130–136.
9. Akple, M. S., Low, J., Qin, Z., Wageh, S., Al-Ghamdi, A. A., Yu, J., et al. Nitrogen-doped TiO_2 microsheets with enhanced visible light photocatalytic activity for CO_2 reduction. *Chinese J. Catal*., 2015, **36**(12), 2127–2134.
10. Civiš, S., Ferus, M., Knížek, A., Kubelík, P., Kavan, L., and Zukalová, M. Photocatalytic transformation of CO_2 to CH_4 and CO on acidic surface of TiO_2 anatase. *Opt. Mater.*, 2015, **56**, 80–83.
11. Fujishima, A. and Honda, K. Electrochemical photolysis of water at a semiconductor electrode. *Nature*, 1972, **238**(5358), 37–38.
12. Hanaor. D. A. H. and Sorrell, C. C. Review of the anatase to rutile phase transformation. *J. Mater. Sci*., 2011, **46**(4), 855–874.
13. Zaman, A. C., Üstündağ, C. B., Kaya, F., and Kaya, C. Synthesis and electrophoretic deposition of hydrothermally synthesized multilayer TiO_2 nanotubes on conductive filters. *Mater. Lett*., 2012, **66**(1), 179–181.
14. Daviðsdóttir, S., Canulescu, S., Dirscherl, K., Schou, J., and Ambat, R. Investigation of photocatalytic activity of titanium dioxide deposited on metallic substrates by DC magnetron sputtering. *Surf. Coatings Technol*., 2013, **216**, 35–45.
15. Oja, I., Mere, A., Krunks, M., Solterbeck, C.-H., and Es-Souni, M. Properties of TiO_2 Films Prepared by the Spray Pyrolysis Method. *Solid State Phenom*., 2004, **99**, 259–264.
16. Varghese, O. K., Gong, D., Paulose, M., Grimes, C. A., and Dickey, E. C. Crystallization and high-temperature structural stability of titanium oxide nanotube arrays. *J. Mater. Chem*., 1998, **8**, 1731–1734.
17. Hasan, M. M., Haseeb, A. S. M. A., Saidur, R., and Masjuki, H. H. Effects of annealing treatment on optical properties of anatase TiO_2 thin films. *Int. J. Mech. Aerosp. Ind. Mechatr. Manuf. Eng.*, 2008, **2**, 410–414.
18. Mor, G. K., Varghese, O. K., Paulose, M., Shankar, K., and Grimes, C. A. A review on highly ordered, vertically oriented TiO_2 nanotube arrays: fabrication, material properties, and solar energy applications. *Sol. Energy Mater. Sol. Cells*., 2006, **90**(14), 2011–2075.
19. Yuangpho, N., Le, S. T. T., Treerujiraphapong, T., Khanitchaidecha, W., and Nakaruk, A. Enhanced photocatalytic performance of TiO_2 particles via effect of anatase–rutile ratio. *Phys. E. Low Dimens. Syst. Nanostruct.,* 2015, **67**, 18–22.
20. Grimes, C. A. and Mor, G. K. 2009. *TiO_2 nanotube arrays*. MA: Springer US, Boston.
21. Regonini, D., Bowen, C. R., Jaroenworaluck, A., and Stevens, R. A review of growth mechanism, structure and crystallinity of anodized TiO_2 nanotubes. *Mater. Sci. Eng. R. Reports*, 2013, **74**(12), 377–406.
22. Roy, P., Berger, S., Schmuki, P., and Schmuki, P. TiO_2 nanotubes: synthesis and applications. *Angew. Chem. Int. Ed*., 2011, **50**, 2904–2939.
23. Kubelka, P. New Contributions to the optics of intensely light-scattering materials. Part I. *J. Opt. Soc. Am*., 1948, **38**(5), 448.
24. Kubelka, P. New contributions to the optics of intensely light-scattering materials. Part II: nonhomogeneous layers. *J. Opt. Soc. Am*., 1954, **44**(4), 330.
25. Cronemeyer, D. C. and Gilleo, M. A. The optical absorption and photoconductivity of rutile. *Phys. Rev*., 1951, **82**(6), 975–976.
26. Scanlon, D. O., Dunnill, C. W., Buckeridge, J., Shevlin, S. A., Logsdail, A. J., Woodley, S. M., et al. Band alignment of rutile and anatase TiO_2. Nat. Mater., 2013, **12**(9), 798–801.
27. Beranek, R. (Photo)electrochemical methods for the determination of the band edge positions of TiO_2-based nanomaterials. *Adv. Phys. Chem*., **2011**, 80–83.
28. Sellers, M. C. K. and Seebauer, E. G. Measurement method for carrier concentration in TiO_2 via the Mott-Schottky approach. *Thin Sol. Films*., 2011, **519**(7), 2103–2110.

Faasijaotuse ramanspektraalne identifitseerimine anoodtitaanoksiidist pinnakatetes

Ainars Knoks, Janis Kleperis ja Liga Grinberga

On uuritud titaani anoodimisel saadud titaandioksiidi faasikoostise ja optiliste ning elektrokeemiliste omaduste sõltuvust anoodimisprotsessi parameetritest. Ramanspektroskoopiliste mõõtmiste tulemused näitasid, et sõltuvalt elektrolüüdi valikust (kas H_3PO_4 või H_2SO_4) on võimalik saada kas anataasi või rutiili faasi ülekaaluga titaandioksiidi. Samuti mõjutas faasikoostist objekti ettevalmistamine anoodimiseks ja anoodimisele järgnenud termotöötlus. Faasikoostis omakorda mõjutas otseselt TiO_2 fotokatalüütilist aktiivsust. Uuringute tulemusena on välja selgitatud fotovoolu ja laengukandjate kontsentratsiooni sõltuvus TiO_2 faasikoostisest.